Am J Physiol Cell Physiol 286: C952–C964, 2004.
First published November 12, 2003; 10.1152/ajpcell.00266.2003.

Changes in cellular composition of kidney collecting duct cells in rats with lithium-induced NDI

Birgitte Mønster Christensen,[1,2] David Marples,[3] Young-Hee Kim,[1,2] Weidong Wang,[1,2] Jørgen Frøkiær,[1,4] and Søren Nielsen[1,2]

[1]*Water and Salt Research Center,* [2]*Institute of Anatomy, and* [4]*Institute of Experimental Clinical Research, University of Aarhus, DK-8000 Denmark; and* [3]*School of Biomedical Sciences, University of Leeds, Leeds LS2 9JT, United Kingdom*

Submitted 26 June 2003; accepted in final form 4 November 2003

Christensen, Birgitte Mønster, David Marples, Young-Hee Kim, Weidong Wang, Jørgen Frøkiær, and Søren Nielsen. Changes in cellular composition of kidney collecting duct cells in rats with lithium-induced NDI. *Am J Physiol Cell Physiol* 286: C952–C964, 2004. First published November 12, 2003; 10.1152/ajpcell.00266.2003.—Lithium treatment for 4 wk caused severe polyuria, dramatic downregulation in aquaporin-2 (AQP-2) expression, and marked decrease in AQP-2 immunoreactivity with the appearance of a large number of cells without AQP-2 labeling in the collecting ducts after lithium treatment. Surprisingly, this was not all due to an increase in AQP-2-negative principal cells, because double immunolabeling revealed that the majority of the AQP-2-negative cells displayed [H^+]ATPase labeling, which identified them as intercalated cells. Moreover, multiple [H^+]ATPase-labeled cells were adjacent, which was never seen in control rats. Quantitation confirmed a significant decrease in the fraction of collecting duct cells that exhibited detectable AQP-2 labeling compared with control rats: in cortical collecting ducts, 40 ± 3.4 vs. 62 ± 1.8% of controls ($P < 0.05$; $n = 4$) and in inner medullary collecting ducts, 58 ± 1.6 vs. 81 ± 1.3% of controls ($P < 0.05$; $n = 4$). In parallel, a significant increase in the fraction of intercalated ([H^+]ATPase-positive) cells was shown. Urine output, whole kidney AQP-2 expression, cellular organization, and the fractions of principal and intercalated cells in cortex and inner medulla returned to control levels after 4 wk on a lithium-free diet following 4 wk on a lithium-containing diet. In conclusion, lithium treatment not only decreased AQP-2 expression, but dramatically and reversibly reduced the fraction of principal cells and altered the cellular organization in collecting ducts. These effects are likely to be important in lithium-induced nephrogenic diabetes insipidus.

nephrogenic diabetes insipidus; aquaporin; exchanger

NEPHROGENIC DIABETES INSIPIDUS (NDI) is characterized by the inability of the kidney to concentrate urine in response to vasopressin. In rare cases, NDI can occur as an inherited disorder, which is due to mutations in the *vasopressin-V_2-receptor* or *AQP2* genes (31, 34, 42). However, most commonly the disease is acquired, and often it occurs as a side effect in humans subjected to different drug treatments. Lithium is widely used for treatment of bipolar affective disorders and is known to cause NDI or urinary-concentrating defects in as many as 40% of patients who take the medication (37). Lithium-induced NDI as well as other acquired forms of NDI (e.g., hypokalemia, hypercalcemia, and postobstructive NDI) have been shown to be associated with a downregulation in aquaporin-2 (AQP-2) protein expression (9, 13, 25, 29, 30, 35). AQP-2 is a vasopressin-regulated water channel that is present in kidney collecting duct principal cells and connecting tubule cells. The mechanism by which lithium inhibits the expression of AQP-2 is not clearly understood. It may inhibit the activity of adenylate cyclase and thus prevent the production of cAMP and subsequently the activity of protein kinase A, which are involved in the regulation of AQP-2 expression as well as vesicular trafficking of AQP-2 (7).

It was previously shown that lithium induces structural changes and affects cell proliferation in kidneys (12, 17, 19). In addition, lithium has effects on both inhibition and stimulation of cell proliferation in other systems. Lithium treatment of nephrectomized rats was shown to cause increased proliferation of neural lobe astrocytes in vivo (26). In contrast, lithium decreased cell proliferation of primary bovine aortic endothelial cells by causing sustained G_2/M cell cycle arrest without affecting cell viability. This effect was partly reversible after lithium cessation (28). In another study, lithium also caused accumulation of HL-60 cells in the G_2/M phase, and this was associated with the onset of apoptosis (27). Aside from having an effect on AQP-2 protein levels, one can hypothesize that lithium may also affect cellular composition in kidney collecting ducts. Indeed, the cellular composition of adult rat kidney collecting ducts was previously shown to be remodeled by chronic carbonic anhydrase inhibition (3). Kidney collecting ducts are composed of principal and intercalated cells. In rat cortical collecting ducts (CCDs), the percentage of principal cells is ~60% (22), and this number increases slightly along the outer and inner stripes of outer medullary collecting ducts; in the proximal part (IM-1) of inner medullary collecting ducts (IMCDs), ~90% of the cells are principal cells. In the middle part of the inner medulla only a very small amount of intercalated cells is found, and no intercalated cells are located in the distal part of the inner medulla. The intercalated cells are involved in acid-base balance, whereas the principal cells are responsible for hormonally regulated sodium and water reabsorption.

In this study, we investigated whether the cellular composition of collecting ducts changes during chronic lithium treatment and whether the effects were reversible after a 4-wk recovery period.

MATERIALS AND METHODS

Experimental Animals and Protocols

These experiments conform to the guidelines of the National Institutes of Health.

Address for reprint requests and other correspondence: S. Nielsen, Water and Salt Research Center, Institute of Anatomy, Univ. of Aarhus, DK-8000 Aarhus, Denmark (E-mail: sn@ana.au.dk).

The costs of publication of this article were defrayed in part by the payment of page charges. The article must therefore be hereby marked "*advertisement*" in accordance with 18 U.S.C. Section 1734 solely to indicate this fact.

Wistar rats were obtained from M & B (Ejby, Denmark). Lithium bicarbonate was solubilized in water and a small amount of hydrogen chloride, and the lithium chloride solution was added to food to yield a lithium concentration of 40 or 60 mmol/kg of dry food as previously described (29).

Protocol 1. In *protocol 1*, rats received food that contained a lithium concentration of 40 mmol/kg of dry food for the first 7 days, and the next 3 wk, the lithium concentration was increased to 60 mmol/kg of dry food ($n = 10$). This protocol was previously shown to result in therapeutic plasma lithium levels (0.8–1.3 mM; Ref. 29). All rats on lithium therapy had access to a sodium chloride block to ensure adequate intake of sodium chloride [and thereby prevent lithium intoxication and a fatal outcome (40)] and also to avoid negative sodium balance. Control rats received normal food ($n = 10$). All rats had free access to water and food.

Protocol 2. In a second protocol, 10 rats were placed on a lithium diet as described above for 4 wk, and 10 rats received normal food. After the 4-wk treatment, half of the lithium-treated rats and half of the control rats were killed ($n = 5$). The remaining rats ($n = 5$) were fed a lithium-free diet and were studied for an additional 4 wk.

During the last part of the experiments, rats were housed in metabolic cages for 3–7 days to measure urine output and osmolality.

Immunocytochemistry

Fixation. In *protocol 1*, both kidneys were perfusion fixed via the abdominal aorta with either PLP (2% paraformaldehyde, 0.01 M $NaIO_4$, 0.075 M L-lysine, 0.0375 M Na_2HPO_4, pH 6.2; for light microscopy; $n = 4$) or 0.1% glutaraldehyde plus 2% paraformaldehyde in 0.1 M cacodylate, pH 7.4 (for immunoelectron microscopy; $n = 5$). The perfusion-fixed kidneys were postfixed for 30 min in 0.1 M sodium cacodylate, pH 7.4, and were subjected to paraffin embedding or cryosubstitution. In *protocol 2*, one kidney was removed for homogenization and immunoblotting before fixation. The other kidney was perfusion fixed in 3% paraformaldehyde in 0.1 M cacodylate, pH 7.4, and after postfixation, kidneys were subjected to paraffin embedding.

Preparation of tissue for light and laser confocal microscopy. Before paraffin embedding was performed, tissue blocks from whole kidneys were dehydrated in a graded series of ethanol (2 h each in 70, 96, and 99%, respectively) and xylene (overnight). Paraffin sections (2-μm thick) were cut on a Leica RM 2126 microtome and dried overnight at 37°C.

SINGLE LABELING. Sections were incubated with affinity-purified polyclonal antibodies against AQP-2 (LL127, 1:10,000 or 1:15,000 dilution, raised to a COOH-terminal peptide of rat AQP-2) or [H^+]ATPase (LL615, 1:100 or 1:200 dilution, raised to a COOH-terminal peptide of the bovine intercalated cell specific 56-kDa subunit of vacuolar [H^+]ATPase, kindly provided by Mark A. Knepper), or anion-exchanger pendrin (1:200 dilution, raised to a COOH-terminal peptide of mouse pendrin). Labeling was visualized by use of horseradish peroxidase-conjugated goat anti-rabbit Ig and 3,3′-diaminobenzidine (DAB).

DOUBLE LABELING. Three different double-labeling experiments were performed as follows: *1*) rabbit polyclonal AQP-2 antibody (LL127, 1:1,000 dilution) and rabbit polyclonal [H^+]ATPase antibody (LL615, 1:200 dilution); *2*) *band 3*-like Cl^-/HCO_3^- exchanger anion exchanger isoform 1 (AE-1, 1:30,000 dilution, kindly provided by Dr. Philip S. Low, Purdue University) and rabbit polyclonal [H^+]ATPase antibody (LL615, 1:200 dilution); and *3*) rabbit polyclonal AQP-4 antibody (LL182, 1:300 dilution, raised to a COOH-terminal peptide of rat AQP-4) and rabbit polyclonal [H^+]ATPase antibody (LL615, 1:200 dilution). Sections were incubated overnight at 4°C with either AQP-2, AE-1, or AQP-4 antibodies before undergoing incubation with horseradish peroxidase-conjugated goat anti-rabbit secondary antibody and visualization by DAB (brown color) as described above. Sections were then incubated in 3.5% H_2O_2 in methanol to remove any remaining peroxidase from the first staining. Sections were incubated overnight at 4°C with [H^+]ATPase antibody before being incubated with horseradish peroxidase-conjugated secondary antibody. For detection of [H^+]ATPase, Vector SG substrate (Vector Laboratories) was used as the chromogen to produce a gray-blue label, which is easily distinguished from the brown label produced by DAB in the first immunolabeling procedure for AQP-2, AE-1, and AQP-4, respectively. The sections were washed with distilled water and counterstained with hematoxylin.

Double labeling was also performed with polyclonal antibodies against rat AQP-2 (LL127, 1:5,000 dilution) and monoclonal antibodies against [H^+]ATPase (E11, 1:300 dilution, raised to a COOH-terminal peptide of the bovine 31-kDa subunit of vacuolar [H^+]ATPase, kindly provided by Stephen Gluck). Labeling was visualized with Alexa 488- and Alexa 546-conjugated secondary antibodies (Alexa 488 anti-rabbit and Alexa 546 anti-mouse, respectively). The polyclonal [H^+]ATPase antibody only labels intercalated cells similar to an antibody raised against a shorter sequence of the vacuolar [H^+]ATPase 56-kDa subunit (32), whereas the monoclonal [H^+]ATPase antibody also stains the brush border and subvillar invaginations of proximal tubules (16).

For both double-labeling procedures, relatively high concentrations of AQP-2 antibody were used to ensure that cells that expressed even very low levels of AQP-2 were detected. Light microscopy was carried out using a Leica DMRE microscope or a Leica DMIRE2 laser confocal microscope.

Preparation of tissue for immunoelectron microscopy. Tissue blocks prepared from the proximal parts of kidney inner medulla and cortex were infiltrated with 2.3 M sucrose for 30 min, mounted on holders, and rapidly frozen in liquid nitrogen. Frozen tissue blocks were subjected to cryosubstitution and Lowicryl HM20 embedding. Cryosubstitution was performed as previously described (33). Ultrathin (80-nm thick) Lowicryl sections were cut on a Reichert Ultracut FCS microtome and were preincubated with 0.05 M Tris·HCl (pH 7.4) with 0.1% Triton X-100 that contained 0.1% sodium borohydride and 0.05 M glycine and were then incubated with identical concentrations of Tris·HCl and Triton X-100 but with 0.2% skimmed milk. The preincubation was followed by incubation with affinity-purified polyclonal antibodies against AQP-2 (LL358, raised to a COOH-terminal peptide of human AQP-2, inner medulla) or [H^+]ATPase (LL615, cortex), and labeling was visualized with goat anti-rabbit IgG conjugated to 10-nm colloidal gold particles. Grids were counterstained with uranyl acetate for 10 min and lead citrate for 5 s.

Length Measurements of Apical Plasma Membrane Domains

Electronic images were taken of whole kidney sections labeled with polyclonal anti-AQP-2 antibody and peroxide-conjugated secondary antibody (4 pictures per rat in each zone). Photomicrographs were imported into CorelDraw software (Corel), and the apical plasma membranes of collecting ducts and connecting tubules were traced using a polyline. This outline was copied, and in the copy the linear sections corresponding to the AQP-2-negative regions were deleted. The micrograph was then deleted, and the remaining lines were exported to Scion Image software (National Institutes of Health), where the total length of the outline and the lengths of the sections corresponding to AQP-2-positive cells were determined.

Quantification of Principal and Intercalated Cells using Anti-AQP-2 and/or Anti-[H^+]ATPase Antibodies

Cell counting was performed on kidney sections that were single labeled with either polyclonal AQP-2 or [H^+]ATPase antibodies and peroxidase-conjugated goat anti-rabbit IgG as well as on sections double labeled with polyclonal AQP-2 and [H^+]ATPase antibodies and peroxidase-conjugated secondary antibodies. Counting was performed either on the microscope or on electronic images taken with a ×25 objective. The numbers of positive (labeled) and negative (un-

labeled) cells with a distinct nucleus were counted. On kidney sections from rats subjected to *protocol 1*, cell counting was performed on sections labeled with either AQP-2 or [H$^+$]ATPase. The counting was performed in cortex, inner stripe of outer medulla (ISOM), and IM-1, and no distinction was made between collecting ducts and connecting tubules. The cell counting on double-labeled sections was performed only in collecting ducts in cortex, ISOM, and IM-1.

In the recovery study (*protocol 2*), counting was performed on collecting duct in cortex and IM-1 on AQP-2-single-labeled sections.

The fractions of AQP-2- and [H$^+$]ATPase-labeled cells as well as nonlabeled cells, respectively, were calculated from the numbers of positive and negative cells divided by the total number of cells counted in each animal. To calculate the fractional increase or decrease, this number was then divided by the mean control value, and the average fractional values in the two respective groups were calculated.

The total numbers of cells counted on AQP-2-single-labeled sections (*protocol 1*) were 1,843 in IM-1, 1,597 in ISOM, and 1,524 in cortex of control animals ($n = 4$) and 2,251 in IM-1, 1,793 in ISOM, and 943 in cortex of lithium-treated rats ($n = 4$). On [H$^+$]ATPase single-labeled sections (*protocol 1*), the numbers were 2,535 in IM-1, 1,543 in ISOM, and 1,976 in cortex of control animals ($n = 4$) and 3,304 in IM-1, 2,410 in ISOM, and 2,119 in cortex of lithium-treated rats ($n = 4$). On double-labeled sections (*protocol 1*), the numbers were 962 in IM-1, 794 in ISOM, and 5,579 in cortex of control animals ($n = 3$) and 1,809 in IM-1, 1,498 in ISOM, and 6,485 in cortex of lithium-treated animals ($n = 4$). In the recovery study (*protocol 2*), the total numbers of counted cells in cortex were 1,995 cells in controls ($n = 4$) and 1,552 cells in recovered animals ($n = 4$); in IM-1, 1,810 cells were counted in controls ($n = 5$) and 2,714 cells were counted in recovered animals ($n = 4$).

Quantification of Pendrin-Positive Intercalated Cells

Cell counting was performed in CCDs of kidney sections single labeled with pendrin and peroxidase-conjugated secondary antibodies. Counting was performed directly on the microscope. The numbers of positive (labeled) and negative (unlabeled) cells with a distinct nucleus were counted, and the fraction of pendrin-labeled cells was calculated from the number of positive cells divided by the total number of cells counted for each animal. The total numbers of cells counted were 3,480 for the control animals ($n = 4$) and 3,409 for the lithium-treated rats ($n = 4$).

Immunoblotting

Whole kidney was homogenized in dissecting buffer (0.3 M sucrose, 25 mM imidazole, and 1 mM EDTA, pH 7.2) that contained the protease inhibitors leupeptin (8.5 μM) and phenylmethylsulfonyl fluoride (1 mM) and the phosphatase inhibitors okadaic acid (100 nM), sodium orthovanadate (1 mM), and sodium fluoride (25 mM). This homogenate was centrifuged in a Beckman L8M centrifuge at 4,000 *g* for 15 min at 4°C to remove nuclei, mitochondria, and any remaining large cellular fragments. Laemmli sample buffer was added to the supernatant, and samples were run in duplicate. One gel was Coomassie stained to ensure that loading in the lanes was consistent, whereas the other was subjected to immunoblotting (*protocol 1*, 60 μg/lane; *protocol 2*, 80 μg/lane). After transfer by electroelution to nitrocellulose membranes, blots were blocked with 5% milk in PBS-T (that contained 80 mM Na_2HPO_4, 20 mM NaH_2PO_4, 100 mM NaCl, 0.1% Tween 20, pH 7.5) for 1 h and incubated with anti-AQP-2 antibody (LL127, serum, 1:3,000 dilution). The labeling was visualized with a peroxidase-conjugated secondary antibody using an enhanced chemiluminescence system (Amersham).

Films were scanned using an AGFA scanner (Arcus II), and the labeling density was quantitated using specially written software (29). AQP-2 labeling in the samples from the experimental animals was calculated as a fraction of the mean control for that film.

Statistical Analyses

Values are presented as means ± SE. Comparisons between groups were made by unpaired *t*-test with equal or unequal variances. *P* values <0.05 were considered significant.

RESULTS

Lithium Increases Urine Output and Decreases Whole Kidney AQP-2 Expression

Consistent with previous results, chronic lithium treatment resulted in severe polyuria (804 ± 45 vs. 24 ± 2 $\mu l \cdot min^{-1} \cdot kg^{-1}$ in controls, $n = 19$; Table 1) and a corresponding decrease in urine osmolality (141 ± 5 vs. 1,779 ± 85 mosmol/kgH_2O, $n = 20$; Table 1). Immunoblotting of whole kidney samples from the present experiment confirmed that the expression of AQP-2 protein was dramatically reduced to 6 ± 2% of controls (100 ± 21%, $n = 5$; $P < 0.05$; not shown) as previously reported (25, 29).

Immunocytochemistry using paraffin-embedded kidney sections confirmed a marked decrease in AQP-2 protein expression in cortex, outer medulla, and proximal and middle parts of inner medulla in lithium-treated rats (Fig. 1). In CCDs, the downregulation of AQP-2 was more pronounced in the inner parts compared with the outer parts. After lithium treatment in outer CCDs, AQP-2 labeling was seen in apical, cytoplasmic, and basolateral domains, whereas the labeling was mainly observed in apical and cytoplasmic domains in the inner parts of CCDs (see Fig. 5*D*). In IMCDs of lithium-treated rats, a considerable amount of AQP-2 labeling was still confined to the apical plasma membrane domains (see Figs. 1*F* and 5*E*), whereas basolateral labeling was markedly reduced in IM-1 areas. Immunoelectron microscopy from IM-1 regions revealed AQP-2 labeling of both the apical plasma membrane and intracellular vesicles in controls (Fig. 2*A*). This was reduced in kidneys from lithium-treated animals where very sparse labeling of the cytoplasm was observed, but there was still some remaining AQP-2 labeling in the apical plasma membrane (Fig. 2*B*).

Table 1. *Functional data for rats treated with protocols 1 and 2*

	Protocol 1		*Protocol 2*	
	Control	Lithium Treatment	Control	Recovery
Body wt, g	416±11 (18)	308±7* (19)	482±18 (5)	427±18 (5)
Urine output, $\mu l \cdot min^{-1} \cdot kg^{-1}$	24±2 (18)	804±45* (19)	19±2 (5)	23±2 (5)
Urine osmolality, mosmol/kgH_2O	1,779±85 (20)	141±5* (20)	2,048±199 (5)	1,857±80 (5)

Values are means ± SE; *n* (in parentheses), no. of rats; *$P < 0.05$.

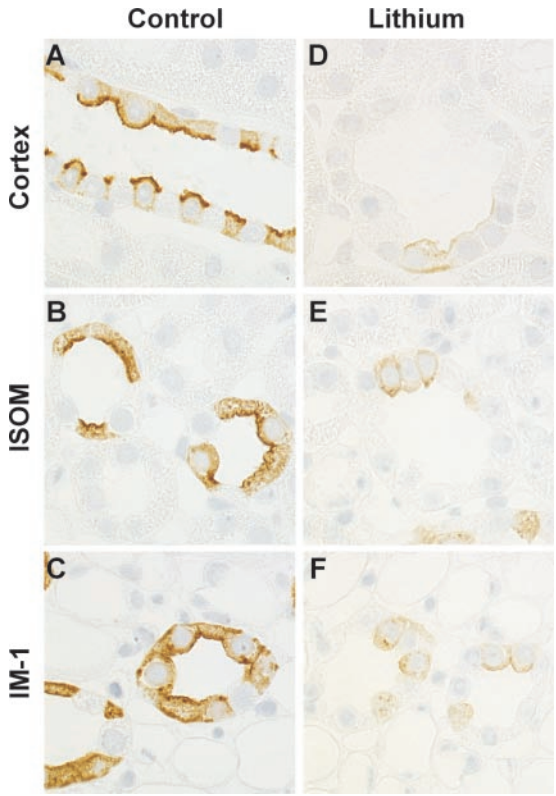

Fig. 1. Immunocytochemistry using whole kidney sections from control (*A-C*) and lithium-treated (*D-F*) rats. Sections were incubated with anti-aquaporin-2 (AQP-2) antibody and peroxidase-conjugated secondary antibody. Expression of AQP-2 was decreased in lithium-treated rats. In multiple collecting duct cells there was no AQP-2 labeling, which indicates that the density of AQP-2-positive cells decreases after lithium treatment. ISOM, inner stripe of the outer medulla; IM-1, proximal part of inner medulla; magnification, ×450.

Lithium Changes Fraction of AQP-2-Labeled Cells in Rat Kidney Collecting Ducts

Kidney collecting ducts are composed of principal and intercalated cells. Principal cells constitute the majority of cells, accounting for ~60% in cortex and outer medulla and ~90% in IM-1. Within inner medulla, only a few intercalated cells are found in the middle part, and none are located in the distal part. As shown in Fig. 1, not only was the expression of AQP-2 decreased, but the fraction of cells labeled for AQP-2 was also decreased in lithium-treated compared with control rats. In particular, long rows of cells without AQP-2 labeling were observed (Fig. 1, *D-F*).

To quantify the decrease in the fraction of AQP-2-labeled cells, the lengths of the apical plasma membrane domains that exhibited AQP-2 labeling and the total lengths of the apical plasma membrane domains in connecting tubules or collecting ducts were measured. There was a significant decrease in the average fraction of the apical surface labeled for AQP-2 in lithium-treated rats (Fig. 3); values for lithium-treated rats vs. control rats were as follows: in cortex, 38 ± 2.2 vs. 78 ± 2.5% ($P < 0.05$; $n = 4$); in ISOM, 52 ± 8.5 vs. 81 ± 2.6% ($P < 0.05$; $n = 4$); and in IM-1, 68 ± 4.4 vs. 87 ± 1.5% ($P < 0.05$; $n = 4$).

These results indicated that there was a decrease in the fraction of AQP-2-positive cells and an increase in the fraction of AQP-2-negative cells after lithium treatment. However, it cannot be ruled out that the increased length of apical plasma membrane domains negative for AQP-2 may just have been due to enlargement of the AQP-2-negative cells. To further examine this, the fractions of AQP-2-positive and -negative cells were determined. The results showed a decrease in the fraction of AQP-2-positive cells and a corresponding increase in the fraction of AQP-2-negative cells in lithium-treated rats compared with control rats. In cortex, the fraction of AQP-2-positive cells was reduced to 66 ± 0.6% of control values (100 ± 2.0%, $n = 4$; $P < 0.05$), and in IM-1, the fraction was reduced to 75 ± 4.8% of control values (100 ± 1.3%, $n = 4$; $P < 0.05$). There was no significant difference in ISOM. Thus lithium treatment decreased the fraction of AQP-2-positive cells, i.e., principal cells, and the results are consistent with an increase in the fraction of intercalated cells.

Lithium Changes Fraction of [H$^+$]ATPase-Labeled Cells in Collecting Ducts

To further investigate whether the apparent increase in the fraction of AQP-2-negative cells was associated with an increase in the number of intercalated cells, sections were labeled for the B_1 subunit of the vacuolar [H$^+$]ATPase that is known to be a marker for intercalated cells (Fig. 4). Immunolabeling demonstrated that the density of [H$^+$]ATPase-labeled cells appears to be increased in kidneys from lithium-treated rats compared with control rats. Inner medulla, which in control rats contains only few intercalated cells, especially exhibited a marked increase in the density of intercalated cells in response to lithium treatment. This was particularly prominent in IM-1 (Fig. 4*F*) as well as the middle part of inner medulla (not shown). The densities of [H$^+$]ATPase-positive and -negative cells were determined. The results showed a significant increase in the fraction of [H$^+$]ATPase-labeled cells in kidney cortex and inner medulla from lithium-treated rats compared with control rats. The values were as follows: cortex, 153 ± 3.9% (100 ± 2.3%, $n = 4$; $P < 0.05$) and IM-1, 204 ± 10.2% (100 ± 5.8%, $n = 4$; $P < 0.05$). No significant difference was observed in ISOM. Thus quantification of AQP-2- and [H$^+$]ATPase-labeled cells, respectively, revealed a significant decrease in the fraction of principal cells in parallel with an increased fraction of [H$^+$]ATPase-positive intercalated cells in cortex and inner medulla. The increase in the fraction of [H$^+$]ATPase-labeled cells is consistent with a lithium-induced increase in [H$^+$]ATPase protein expression as shown by immunoblot studies using a slightly different protocol (40 mmol lithium/kg of dry food for 4 wk; Ref. 23).

Double Labeling with Anti-AQP-2 and Anti-[H$^+$]ATPase

To confirm the changes in cellular composition after lithium treatment and to investigate whether any cells in the lithium-treated animals labeled either positive or negative for both AQP-2 and [H$^+$]ATPase, double labeling was performed with polyclonal AQP-2 and monoclonal [H$^+$]ATPase (Fig. 5, *A*, *B*, *D*, and *E*) using an immunofluorescence method as well as with polyclonal AQP-2 and polyclonal [H$^+$]ATPase using horseradish peroxidase immunolabeling (Fig. 5, *C* and *F*). The results revealed long rows of [H$^+$]ATPase-labeled cells in lithium-treated rats (Fig. 5, *D-F*), which were never seen in control rats. The changes in cellular composition were further confirmed via cell counting on the sections double labeled with

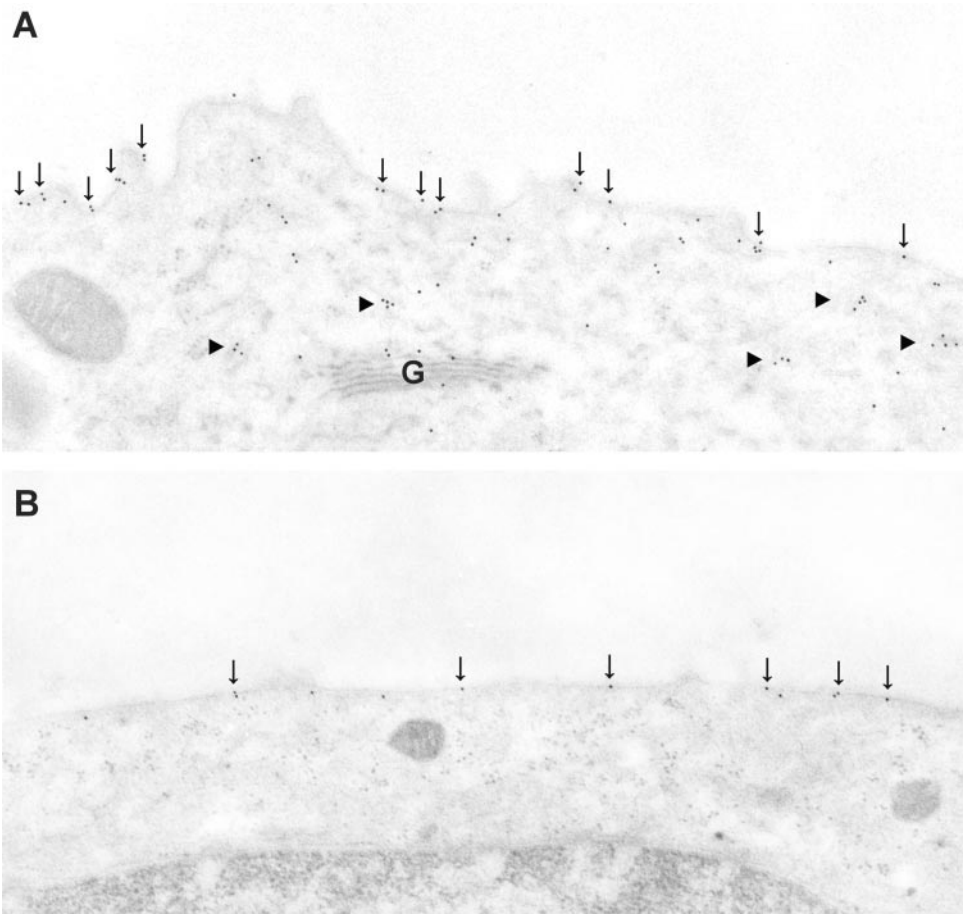

Fig. 2. Electron micrographs of ultrathin Lowicryl sections from kidney inner medulla of a control (*A*) and a lithium-treated (*B*) rat. Sections were immunogold labeled for AQP-2. In control rat, extensive labeling was associated with the apical plasma membrane (arrows) and intracellular vesicles (arrowheads). After lithium treatment, no or very sparse labeling of the intracellular vesicles was observed. AQP-2 labeling was confined to the apical plasma membrane. G, Golgi apparatus; magnification, ×31,200.

polyclonal AQP-2 and polyclonal [H$^+$]ATPase (Fig. 5, *C* and *F*). The results showed a significant decrease in the fraction of AQP-2-positive cells and a corresponding increase in the fraction of [H$^+$]ATPase cells in CCDs and IMCDs in the lithium-treated rats compared with control rats (Table 2). In the distal part of CCDs, the effect was more pronounced, whereas in the proximal part of CCDs, the distributions of AQP-2- and [H$^+$]ATPase-labeled cells were more similar to those of control rats. Similar to the single-labeling results, there were no statistical differences in ISOM between lithium-treated and control rats (Table 2).

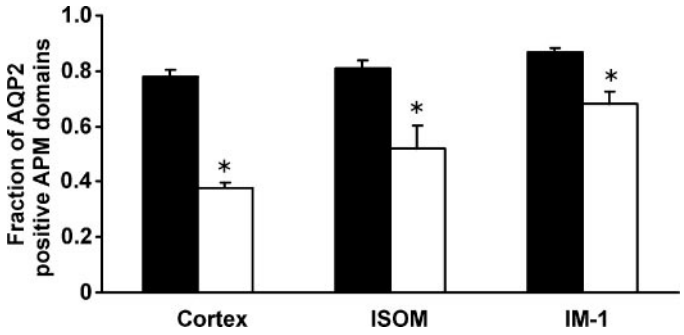

Fig. 3. Measurements of the fractions of apical plasma membrane (APM) domains positive for AQP-2 in control (filled bars) and lithium-treated (open bars) rats. Length of the apical plasma membrane surface in the AQP-2-labeled cells as well as the total lengths of the apical plasma membrane domains of labeled and unlabeled cells were measured in cortex, ISOM, and IM-1. Average fraction of the apical surface labeled for AQP-2 was determined. There was a significant decrease in the apical surfaces labeled for AQP-2 in all three zones in the lithium-treated animals. *$P < 0.05$.

Quantitation of the double-labeled sections revealed that 10% of the cells in CCDs were negative for both AQP-2 and [H$^+$]ATPase in lithium-treated rats (Fig. 5, *D* and *F*, arrows, and Table 2). Whether these cells are principal cells with no AQP-2 expression or undetectable levels of AQP-2 (despite the high antibody concentration used) or intercalated cells with no [H$^+$]ATPase expression is not known. Even if the negative cells are principal cells, the fraction of principal cells was still significantly decreased in CCDs of lithium-treated rats compared with control rats (51 ± 1.6 vs. 62 ± 1.7%, $n = 4$; $P < 0.05$). In inner medulla, the fraction of completely negative cells was very low in lithium-treated rats and was not statistically different from controls. In very rare cases (<1%), it was not possible to determine whether a cell was labeled or not.

The double labeling also showed that cells were almost exclusively positive for only one of the proteins, and only very occasionally did cells appear to stain positive for both AQP-2 and [H$^+$]ATPase (Fig. 5*D*, arrowhead). This was the case in kidneys from both control and lithium-treated rats.

[H$^+$]ATPase-Positive Cells Were Costained with AE-1 but Not with AQP-4

To obtain additional evidence that the increased fraction of [H$^+$]ATPase-positive cells in IM-1 after lithium treatment

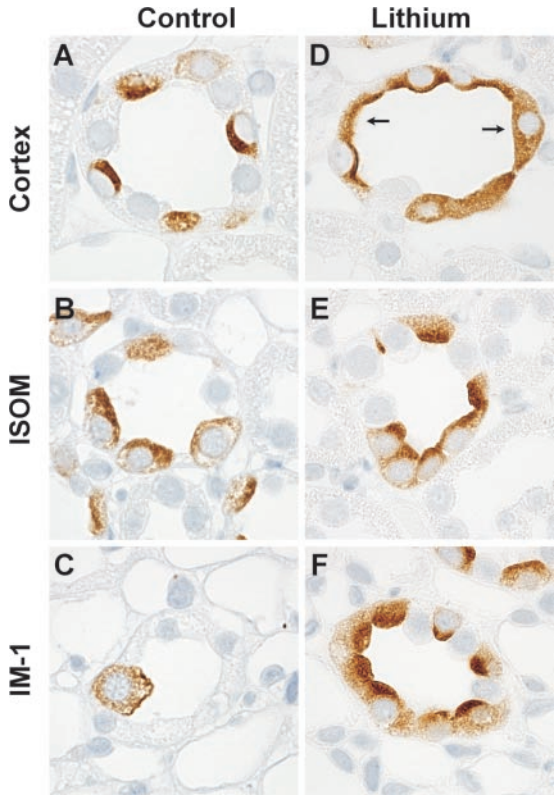

Fig. 4. Immunocytochemistry using whole kidney sections from control (*A-C*) and lithium-treated (*D-F*) rats. Sections were incubated with anti-[H^+]ATPase antibody and peroxidase-conjugated secondary antibody. Density of [H^+]ATPase-positive cells appeared to be increased in the lithium-treated rats. Strikingly, rows of [H^+]ATPase-positive cells were observed in these rats that were not present in control rats. In cortex, some of the [H^+]ATPase cells appeared more flattened (arrows). Magnification, ×600.

comprised intercalated cells, sections from paraffin-embedded kidneys were double labeled with anti-[H^+]ATPase and an antibody that recognizes the *band 3*-like Cl^-/HCO_3^- exchanger AE-1, which is known to label the basolateral plasma membrane of type A intercalated cells. In inner medulla, where the increase of the density of [H^+]ATPase-positive cells was most pronounced, all [H^+]ATPase-positive cells showed basolateral AE-1 staining, which indicates they were type A intercalated cells (Fig. 6*A*). We have recently shown via immunoblotting that AE-1 protein expression is increased in inner medulla after lithium treatment, which is consistent with the present results (23). As described, double labeling with AQP-2 and [H^+]ATPase showed that virtually no cells were stained with both antibodies, and this was further confirmed by double labeling with antibodies against [H^+]ATPase and AQP-4. AQP-4 was not present in any of the [H^+]ATPase-positive cells in IMCDs (Fig. 6*B*) or in the rest of the collecting ducts.

Thus the increased fraction of [H^+]ATPase-positive cells in IMCDs after lithium treatment appeared to be intercalated cells. This was also further supported by immunoelectron microscopy to show that the adjacent [H^+]ATPase-labeled cells in inner medulla have same ultrastructural characteristics as type A intercalated cells [using 40 mmol lithium/kg of dry food for 4 wk (23) and the present protocol, not shown].

No Changes in Fraction of Pendrin-Labeled Cells After Lithium Treatment

To investigate whether there were any different responses to lithium treatment in the subtypes of intercalated cells, we performed immunolabeling of the Cl^-/HCO_3^- exchanger pendrin and cell counting of pendrin-positive cells (Fig. 7). It was previously demonstrated that pendrin is a Cl^-/HCO_3^- exchanger that is only expressed in the apical plasma membrane domains of type B intercalated cells and non-A/non-B intercalated cells (24). No pendrin-labeled cells were observed in inner medulla of either control or lithium-treated rats (not shown). In CCDs there was no significant difference in the fraction of pendrin-labeled cells between the control and lithium-treated animals (controls, 23 ± 1.0 vs. 24 ± 7.3%, $n = 4$; P = not significant). Consistent with this, previous immunoblot analysis has shown an unchanged expression of pendrin in cortex in response to lithium treatment (23).

Ultrastructure of Types A and B Intercalated Cells in Lithium-Treated Rats

In the present study, all intercalated cells with [H^+]ATPase in the inner medulla of lithium-treated rats had the same ultrastructural characteristic of type A intercalated cells, which is consistent with the previous report by Kim et al. (23). Immunoelectron microscopy of kidney cortex demonstrated that compared with the normal configuration of type A intercalated cells in control rats (Fig. 8), the majority of the adjacent type A intercalated cells from lithium-treated rats were more flattened and elongated (Fig. 9, *A* and *C*). The type A intercalated cells in the control animals had apical microplicae and numerous mitochondria in the cytoplasm (see Fig. 8*A*) as well as [H^+]ATPase labeling in the apical plasma membrane (see Fig. 8*B*). Aside from having a more elongated cytoplasm, the adjacent type A cells of lithium-treated rats also had fewer microplicae and mitochondria than control rats. In some cells apical [H^+]ATPase labeling was seen (Fig. 9*B*), whereas in other cells the labeling was mainly observed in the subapical region of the cells (Fig. 9*D*).

Immunoelectron microscopy confirmed that the density of the type B intercalated cells was not altered. Similar to type B cells of control rats (Fig. 10), the ultrastructure of type B cells in lithium-treated rats (Fig. 11) was characterized by a few apical microprojections and denser cytoplasm than in type A cells. The cells contained [H^+]ATPase in the basolateral membrane and cytoplasm, and there were no differences between control and lithium-treated rats in the distribution and density of [H^+]ATPase in type B cells.

Four-Week Recovery Period Reverses AQP-2 Expression and Cellular Profiles to Control Levels

To investigate whether the lithium effects were reversible, rats were allowed to recover on a lithium-free diet for 4 wk after lithium treatment (*protocol 2*). Urine-output measurements (23 ± 2 vs. 19 ± 2 $\mu l \cdot min^{-1} \cdot kg^{-1}$ in lithium-treated and control rats, respectively, $n = 5$; see Table 1) and the corresponding urine osmolality values (1,857 ± 80 vs. 2,048 ± 199 mosmol/kgH_2O in lithium-treated and control rats, respectively, $n = 5$; see Table 1) returned to levels that were not significantly different from control animals. Immunoblotting of

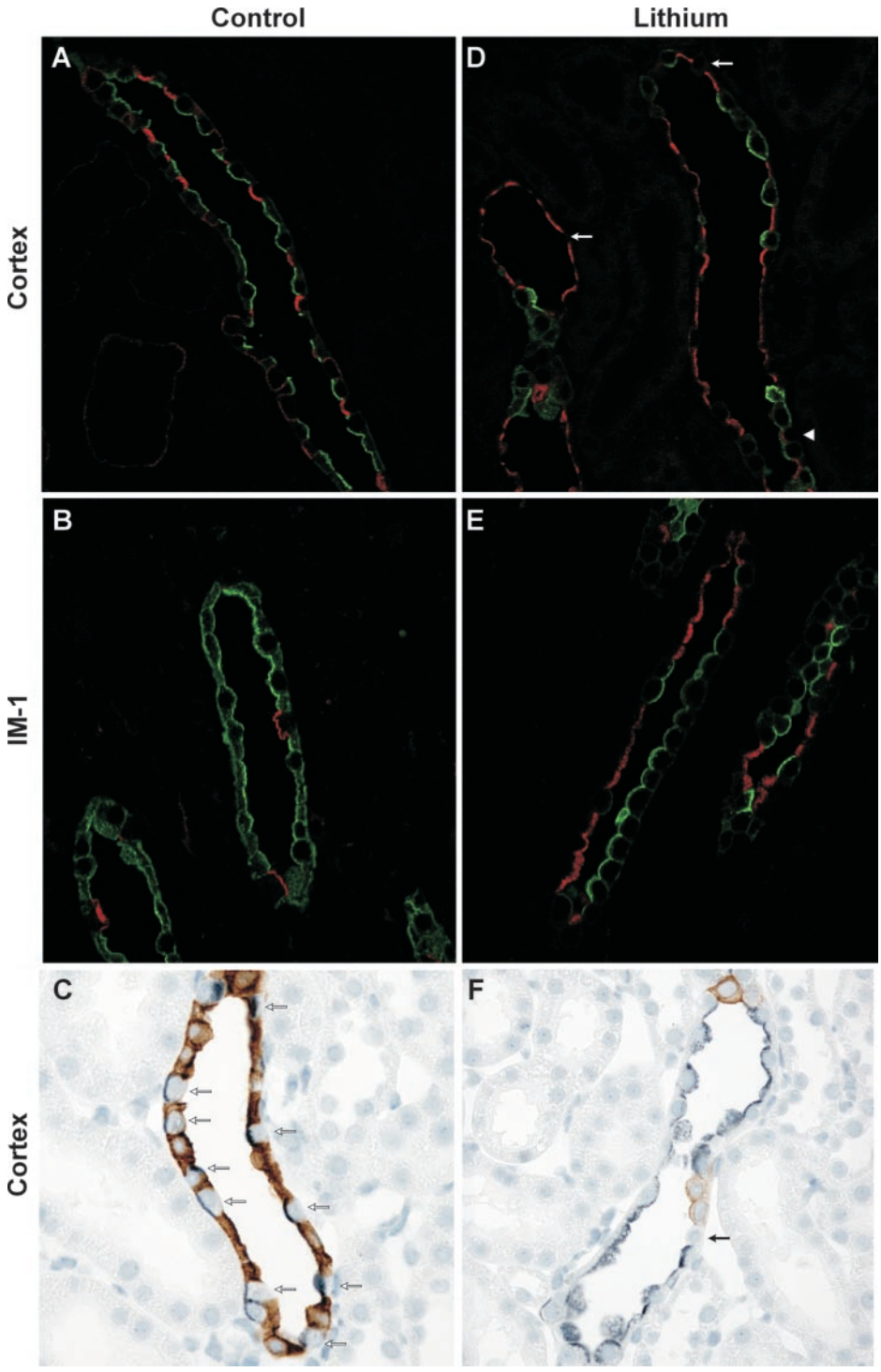

Fig. 5. Double labeling of whole kidney sections (cortex and IM-1) from control (*A–C*) and lithium-treated (*D–F*) rats. Fluorescent double labeling was performed with polyclonal anti-AQP-2 antibody (using a relatively high concentration; green) and monoclonal anti-[H$^+$]ATPase antibody (red). Labeling was visualized by Alexa 488- and Alexa 546-conjugated secondary antibodies (*A–B* and *D–E*). Double labeling with peroxidase-conjugated secondary antibody was performed with polyclonal primary antibodies (*C* and *F*), anti-AQP-2 antibody (brown), and polyclonal anti-[H$^+$]ATPase antibody (gray-blue). In both cortex and IM-1, an increased density of [H$^+$]ATPase-positive cells was observed after lithium treatment (*D–F*) compared with controls (*A–C*, open arrows). In general, very few cells stained positive for both AQP-2 and [H$^+$]ATPase (*D*, arrowhead). In cortex, some cells were negative for both AQP-2 and [H$^+$]ATPase (*D* and *F*, arrows). Magnification, ×300 (*A-D*) and ×375 (*E* and *F*).

whole kidney samples prepared from recovered animals and corresponding control rats showed that AQP-2 protein levels returned to control levels (95 ± 15 vs. 100 ± 29%, $n = 5$; P = not significant; Fig. 12). The density values and distributions of AQP-2-positive cells were also similar to control rats as shown by immunocytochemistry (Fig. 13). Quantitation of AQP-2-labeled cells in CCDs and IM-1s showed that there were no significant differences in the fraction of AQP-2-positive cells between the two groups (Fig. 14); values were as follows: cortex, 60 ± 1.5 vs. 62 ± 1.3% in controls ($n = 4$; P = not significant) and IM-1, 79 ± 5.5 vs. 92 ± 1.3% in controls ($n = 4$; P = not significant). Thus the fractional decrease in principal cells and the fractional increase in intercalated cells, respectively, reversed to control levels after lithium-treated rats had recovered for 4 wk.

DISCUSSION

In this study, AQP-2 protein levels were severely downregulated in rats with lithium-induced NDI, which is consistent

Table 2. *Fraction of AQP-2 and [H$^+$]ATPase-labeled cells in control and lithium-treated animals*

	Control, %	Lithium Treatment, %
Cortex/CCD		
AQP-2	62±1.8	40±3.4*
[H$^+$]ATPase	38±1.7	50±2.0*
Negative	0.1±0.07	10±2.1*
ISOM		
AQP-2	61±4.1	59±4.9
[H$^+$]ATPase	36±4.2	39±4.6
Negative	2.3±1.9	1.6±0.7
IM-1		
AQP-2	81±1.3	58±1.6*
[H$^+$]ATPase	18±1.3	42±1.6*
Negative	0.2±0.1	0.06±0.03

Values are means ± SE; $n = 4$ lithium-treated rats or 3 control rats. Fractions of cells with a distinct nucleus and immunoreactivity for aquaporin-2 (AQP-2) and [H$^+$]ATPase and cells negative for AQP-2 and [H$^+$]ATPase were counted on double-labeled sections. CCD, cortical collecting duct; ISOM, inner stripe of outer medulla; IM-1, proximal part of inner medulla. *$P < 0.05$.

with previous studies (25, 29). Interestingly, quantitation of cells revealed a marked decrease in the fraction of collecting duct cells that exhibited detectable AQP-2 labeling and an increase in the fraction of AQP-2-negative cells in cortex and inner medulla compared with control rats. Surprisingly, the majority of the AQP-2-negative cells displayed significant [H$^+$]ATPase labeling, thereby identifying them as intercalated cells. This was further confirmed with double labeling using [H$^+$]ATPase and AE-1. In particular, multiple [H$^+$]ATPase-labeled cells were connected, and quantitation revealed an increase in intercalated cell density parallel to the decrease in principal cells. Urine output, whole kidney AQP-2 expression, and fractions of principal and intercalated cells in cortex and inner medulla returned to control levels after a 4-wk recovery period.

The mechanisms behind the changes in the cellular profile in response to lithium and the observed reversibility after lithium cessation are not known. Potential explanations are discussed here.

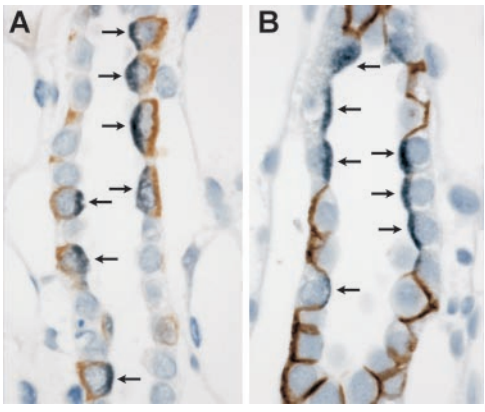

Fig. 6. Double labeling with peroxidase-conjugated secondary antibody of whole kidney sections (IM-1) from lithium-treated rats. Double labeling was performed with polyclonal primary antibodies that recognize anion exchanger isoform 1 (AE-1; brown) and [H$^+$]ATPase (gray-blue; *A*) or with polyclonal primary antibodies that recognize AQP-4 (brown) and [H$^+$]ATPase (gray-blue; *B*). Basolateral AE-1 staining was observed in all cells that contained [H$^+$]ATPase (always apical staining), which identifies them as type A intercalated cells (*A*, arrows). AQP-4 was only present in the [H$^+$]ATPase-negative cells, i.e., principal cells, and not in cells that contained [H$^+$]ATPase labeling (*B*, arrows). Magnification, ×360 (*A*) and ×430 (*B*).

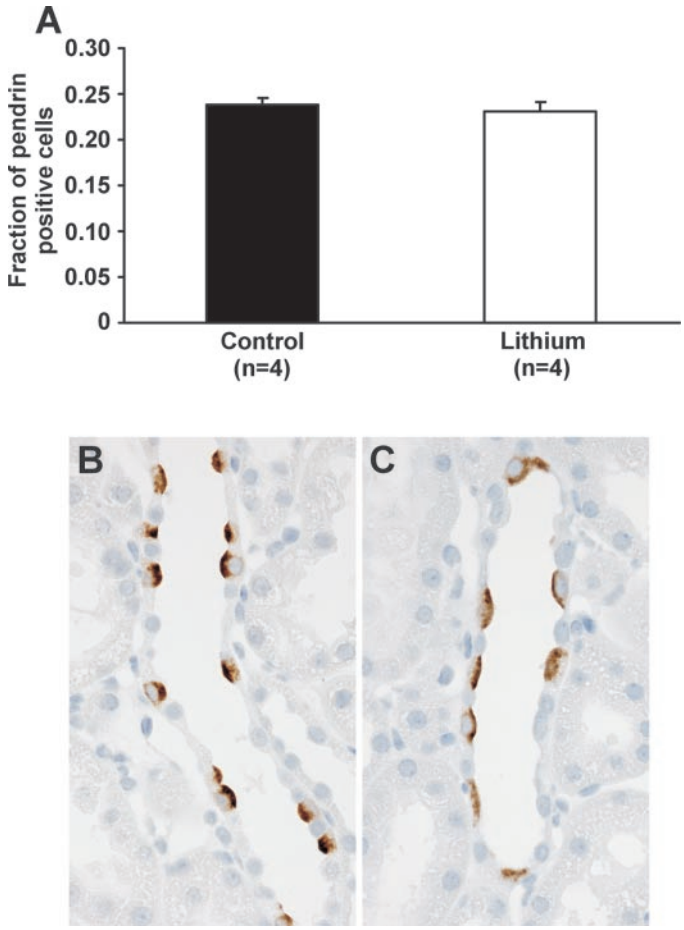

Fig. 7. Quantitation of pendrin-labeled cells in cortex of control and lithium-treated (*A*) rats. Fractions of pendrin-positive and -negative cells were determined on kidney sections from control (*B*) and lithium-treated (*C*) rats. Pendrin was used as a marker for type B intercalated cells and type non-A/non-B intercalated cells. There were no significant differences in the fractions of pendrin-positive cells between the two groups in the cortical collecting duct. Magnification, ×300.

Cellular Profile of Collecting Duct Changed Dramatically in Response to Lithium

Under normal conditions, collecting duct cells in the mature kidney divide at a very slow rate, i.e., the turnover is slow (43). However, an early study from 1982 showed that lithium treatment of rats (using 40 mmol lithium/kg of dry food for 3, 7, and 21 days) can cause an increase in the mitotic rate in the collecting duct cells as shown by [^{3}H]thymidine incorporation (determined after 7 days). In that study, the investigators showed that the hyperplasia and marked increase in DNA synthesis in the collecting ducts seen after lithium treatment were most pronounced at the border region between outer and inner medulla (19). Although they made no distinction between intercalated and principal cells, this study supports our results that show the most marked increase in the number of intercalated cells in the initial and middle parts of IMCD. In another study, lithium also caused accumulation of HL-60 cells in the G_2/M cell phase, and this was associated with the onset of

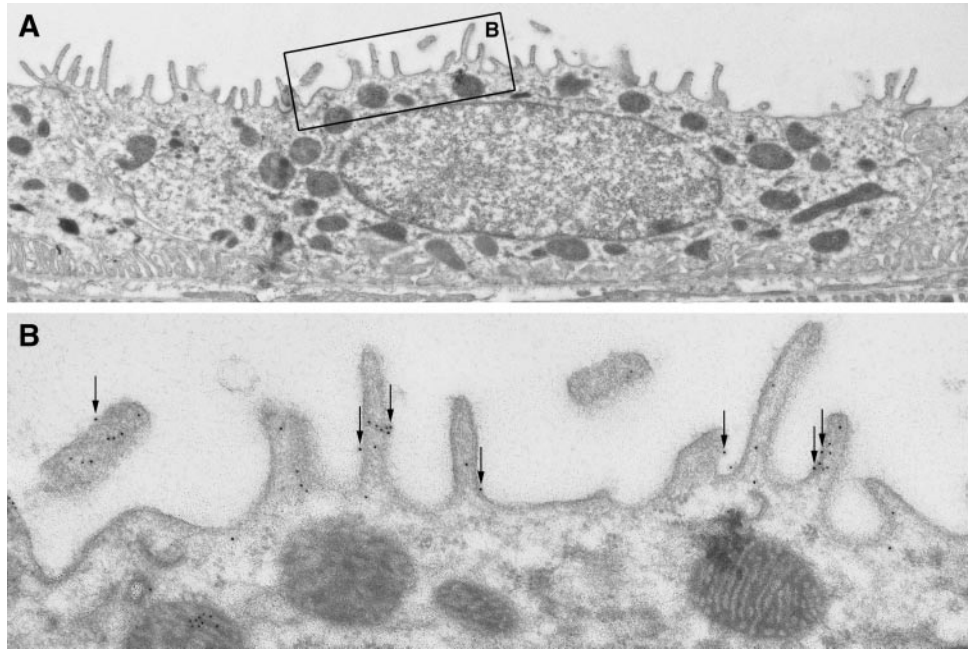

Fig. 8. Electron micrographs of ultrathin Lowicryl sections from cortex of a control rat (*A* and *B*). Sections were immunogold labeled for [H^+]ATPase. In control rats, type A intercalated cells had apical microplicae and numerous mitochondria in the cytoplasm (*A*) as well as [H^+]ATPase labeling in the apical plasma membrane (*B,* arrows). Magnification, ×8,200 (*A*) and ×38,400 (*B*).

apoptosis (27). Therefore, there could be several possible ways to explain the changes in cell composition in kidneys of lithium-treated rats. First, we could speculate that with lithium treatment, intercalated cells may divide faster than principal cells and lead to an increased fraction of intercalated cells. It is also possible that lithium has no effect on the turnover of principal cells but causes the proliferation of intercalated cells only. In addition, lithium treatment could lead to a selective depletion of principal cells, e.g., by apoptosis followed by increased proliferation mainly of intercalated cells. Lithium may also cause apoptosis of principal cells that then leads to increased proliferation of the remaining principal cells and differentiation to both principal and intercalated cells. It is noteworthy that there were ~10% of cells without both AQP-2 and [H^+]ATPase in CCDs of lithium-treated rats, and this percentage was significantly higher than in control rats (as demonstrated in RESULTS). Therefore, there might be more cells undergoing mitosis and/or apoptosis in response to lithium treatment. In fact, there has been no conclusion regarding the origination of principal and intercalated cells in the kidney. Some cell culture and morphological studies suggest that intercalated cells originate from principal cells or some undifferentiated precursor cells (1, 20). Other cell culture studies suggest that β-intercalated cells can give rise to both α-intercalated cells and principal cells, but that principal cells cannot convert to intercalated cells (11). Therefore, additional studies are warranted.

In the present study, we would have expected to see some cells with both AQP-2 and [H^+]ATPase if cell conversion had occurred between principal and intercalated cells. However, the double-labeling results showed that only very few cells from lithium-treated rats stained positive for both AQP-2 and [H^+]ATPase, and some of these rare events may not have been due to true double-labeled cells but rather may have reflected the sectioning and staining of two different cells. The ultrastructural organization of principal and intercalated cells may lead to labeling of the apical part of the principal cell and labeling of the cytoplasm of an underlying intercalated cell with an apical part that does not show in that particular section. Thus the very few double-labeled cells speak against interconversion. Furthermore, we observed the same results from the double labeling with antibodies against AQP-4 and [H^+]ATPase. However, it cannot be ruled out that a potential interconversion between principal and intercalated cells may not occur progressively during the 4-wk treatment period but may take place at an earlier stage during treatment, and a cell converting to another cell type may therefore not be visible after 4 wk of treatment. Interconversion could also explain that the situation reverses after cessation of lithium, i.e., the intercalated cells convert back to principal cells. Thus there are no data in the present study that support interconversion, but it cannot be ruled out entirely.

Whether the observed changes in cellular composition of the collecting ducts represent a direct effect of lithium or are instead due to the side effect of lithium treatment has not been established. It has been suggested that a rise in intracellular sodium can induce cell proliferation of renal epithelial cells with sodium acting as a mitogen (36). Lithium-treated rats exhibit natriuresis (25), and competing lithium uptake by the cells inhibits sodium reabsorption in these rats. It could be speculated that lithium can act as a mitogen. It may also be caused by an indirect effect of lithium treatment, e.g., due to the high vasopressin concentration that is known to be present in lithium-treated animals (2, 4, 15, 38). Vasopressin has been shown to stimulate mesangial cell proliferation (14). It could also be hypothesized that the very high urine flow observed in lithium-treated rats could cause the observed changes in cellular composition. In this regard, it is noteworthy that sustained hyposmotic stress induces cell death in human kidney tubule cells (18). However, Brattleboro rats, which have urine production that is similar to lithium- and furosemide-treated rats (which are also polyuric, although not to the same extent as lithium-treated rats), do not display dramatic changes in cellu-

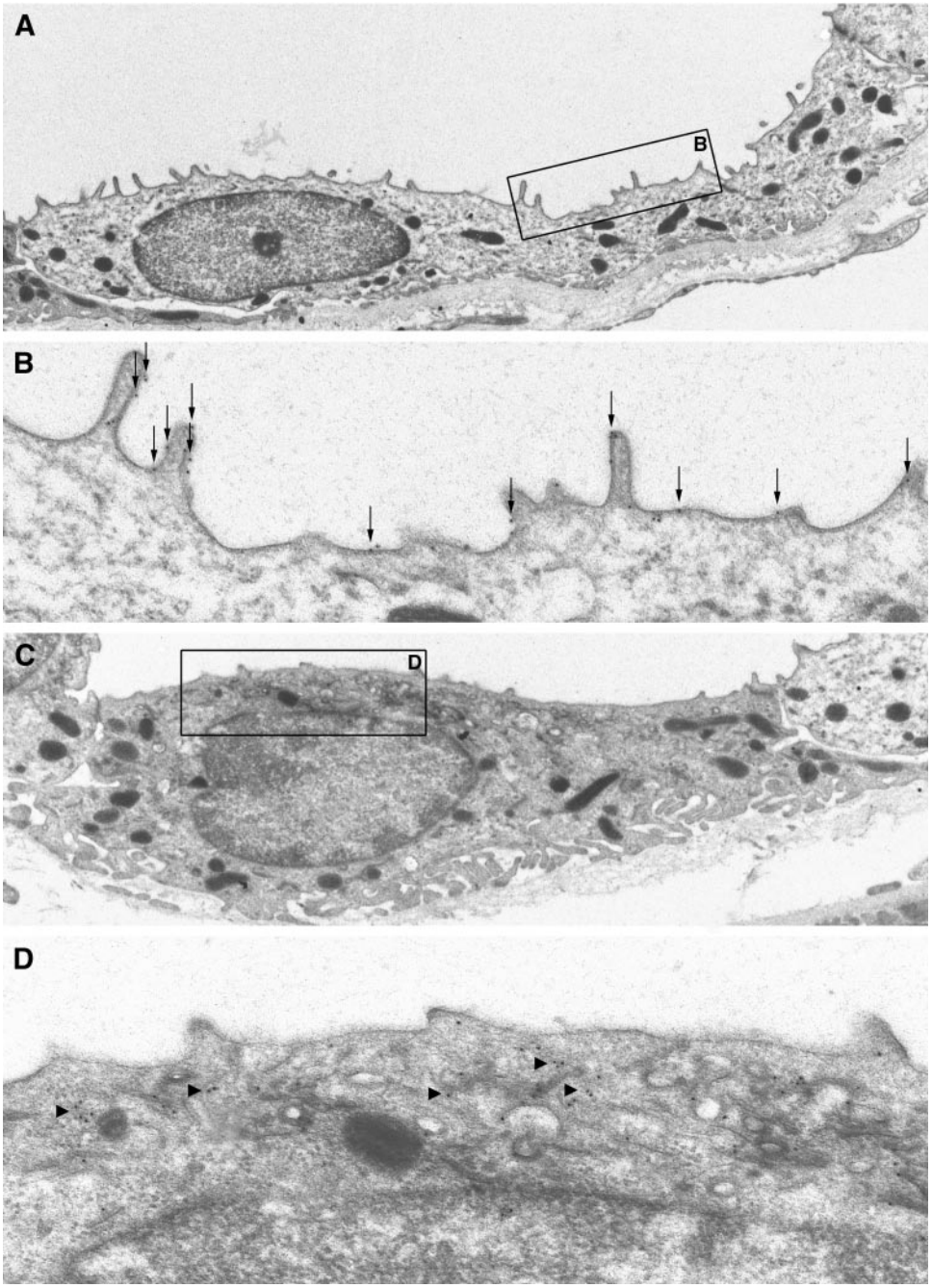

Fig. 9. Electron micrographs of ultrathin Lowicryl sections from cortex of a lithium-treated rat (*A*-*D*). Sections were immunogold labeled for [H^+]ATPase. Two adjacent type A intercalated cells are shown (*A* and *C*). Many of the type A intercalated cells that appeared in rows in cortex had a more elongated cytoplasm and were more flattened than the characteristic type A intercalated cells from the controls (*A* and *C*). They also had fewer microvilli and mitochondria. Some cells were labeled with [H^+]ATPase in the apical plasma membrane (*B*), whereas in other cells, [H^+]ATPase labeled mainly subapically (*D*). Magnification, ×8,400 (*A*); ×41,300 (*B*); ×11,500 (*C*); ×44,500 (*D*).

lar composition (B. M. Christensen and S. Nielsen, unpublished observations).

In several previous studies, investigators showed that lithium causes an acidification defect by decreasing the favorable electric gradient for hydrogen ion secretion and also has an inhibitory effect on the hydrogen ion pump (8). In addition, we have demonstrated in a recent study that in chronic lithium-treated rats, the [H^+]ATPase (B_1 subunit) protein expression and the density of cells with [H^+]ATPase expression were significantly increased (23). Therefore, it can be speculated that the distal renal tubular acidosis induced either by reduced lumen negative transepithelial potential or decreased [H^+]ATPase activity causes the increase of intercalated cells in the kidney, especially in the inner medulla. However, the mechanism behind the increased number of intercalated cells in the inner medulla in response to chronic lithium treatment is not yet established.

The cellular profile of kidney collecting ducts has recently been shown to be remodeled in another animal model, i.e., in adult rats treated with acetazolamide, which inhibits carbonic anhydrase activity (3). The authors speculated that the changes in intercalated cells may be adaptive processes that tend to correct or stabilize the metabolic acidosis that would otherwise ensue after systemic carbonic anhydrase inhibition (3).

Several factors may contribute to the severe polyuria that was observed in lithium-treated rats. The dramatic downregulation of AQP-2 expression and the subsequent reduced

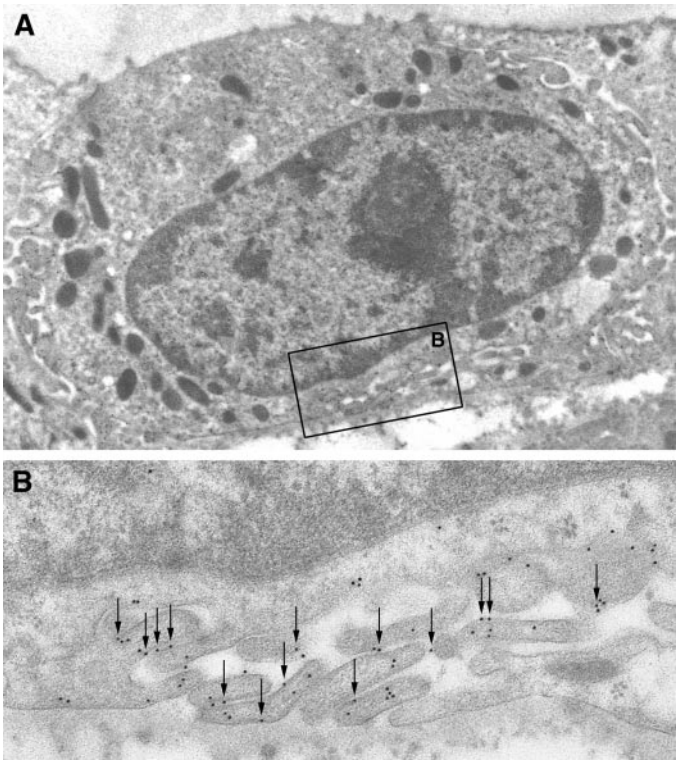

Fig. 10. Electron micrographs of ultrathin Lowicryl sections of a type B intercalated cell from the cortex of a control rat (*A* and *B*). Sections were immunogold labeled for [H^+]ATPase. Type B intercalated cells had fewer apical microprojections and more mitochondria in cytoplasm than the type A intercalated cell (*A*). [H^+]ATPase labeling was seen in the basolateral plasma membrane and also in the cytoplasm (*B*). Magnification, ×9,800 (*A*) and ×42,000 (*B*).

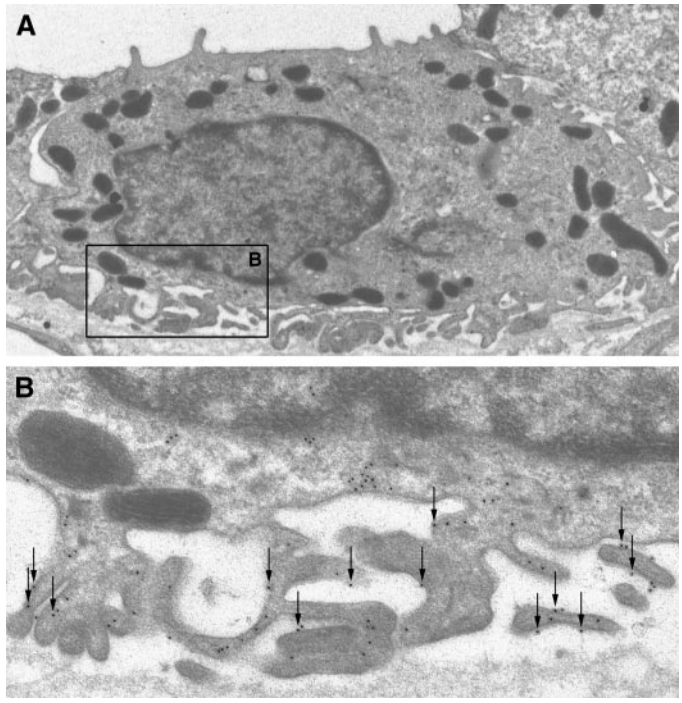

Fig. 11. Electron micrographs of ultrathin Lowicryl sections of a type B intercalated cell from the cortex of a lithium-treated rat (*A* and *B*). Sections were immunogold labeled for [H^+]ATPase. Type B intercalated cells in the lithium-treated rat had a similar ultrastructure as the type B intercalated cells observed in the controls (*A*). Localization and density of [H^+]ATPase labeling was similar to controls (*B*). Magnification, ×10,300 (*A*) and ×34,600 (*B*).

amount of AQP-2 in the apical plasma membrane play a key role. This correlates with the fact that lithium is able to inhibit adenylate cyclase activity and thus the production of cAMP. AQP-2 expression in basolateral plasma membrane domains in IM-1 appeared to be decreased after lithium treatment. The role of AQP-2 in the basolateral plasma membrane is not known, but the decreased expression of AQP-2 in basolateral plasma membrane domains in this part of the inner medulla may potentially also contribute to the polyuria. There have been several reports regarding the role of vasopressin on basolateral AQP-2 targeting. We have recently shown that acute V_2-receptor agonist treatment of Brattleboro rats did not cause an increase in basolateral AQP-2 expression, and similarly, acute V_2-receptor antagonist treatment did not cause a retrieval of AQP-2 from the basolateral plasma membrane, which suggests that basolateral AQP-2 is probably not regulated by short-term vasopressin stimulation (6). However, van Balkom et al. (41) recently showed that acute vasopressin stimulation of dissected kidney slices from normal rats induced insertion of AQP-2 into basolateral plasma membrane domains in the distal part of inner medulla.

AQP-3 is present in the basolateral plasma membrane of collecting duct principal cells, where it functions as an exit pathway for water entering through AQP-2 in the apical plasma membrane. AQP-3 protein expression has previously been shown to be downregulated to the same extent as AQP-2 in whole kidney preparations from lithium-treated rats, and the density of AQP-3 labeling in the basolateral plasma membrane in inner medulla was decreased after lithium treatment (25). Thus the decrease in AQP-3 expression probably contributes to the marked diuresis. Transport of AQP-3 to the basolateral plasma membrane is apparently not regulated by vasopressin, because only a very small

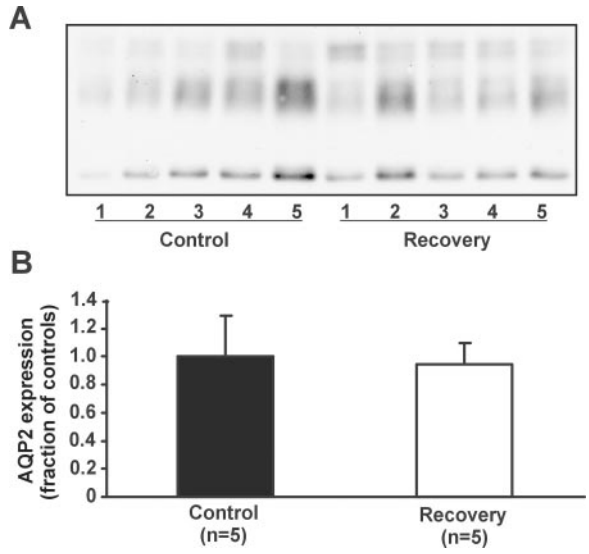

Fig. 12. Immunoblot (*A*) of AQP-2 in kidney of control rats and rats treated with lithium for 4 wk followed by a 4-wk recovery period and corresponding densitometric analysis (*B*). AQP-2 serum recognizes 29-kDa and 35- to 50-kDa bands that correspond to nonglycosylated and glycosylated forms of AQP-2. There were no significant differences in AQP-2 protein levels between the two groups.

proportion of AQP-3 is present in intracellular vesicles in normal rats (10). In contrast, AQP-3 appears to be regulated by vasopressin on a long-term basis (39). Another key factor in the development of polyuria may be the fractional reduction in principal cells observed after lithium treatment. Thus the decrease in water reabsorption is probably a combination of the reduced fraction of AQP-2-containing cells and the decrease in AQP-2 expression in the remaining principal cells.

In conclusion, the decreased fraction of principal cells in parallel with the increased fraction of intercalated cells observed in this study are likely to be important in lithium-induced NDI. Additional investigations are needed to clarify the mechanisms behind these major changes in cell composition in renal collecting ducts.

Recovery from Lithium-Induced NDI

Both urine output and AQP-2 protein levels returned completely to control levels 4 wk after cessation of lithium treatment. A previous experiment where rats were treated with lithium for 35 days showed that after 7 days of recovery, rats had increased their AQP-2 expression incompletely to 40% of control levels (29). The recovery of patients after lithium therapy is also slow. The urinary concentrating ability improves significantly during the first 2 mo after removal of lithium. However, 17 out of 27 patients had persistent concentrating defects 1 yr after stopping lithium (5). In the present study, there were no significant differences in the fraction of AQP-2-positive cells between the recovered animals and the control animals after 4 wk of recovery. Moreover, the cellular profile reverted to the normal configuration, i.e., the long rows of intercalated cells seen in the lithium-treated rats were no longer visible, and collecting duct intercalated cells were almost exclusively separated from other intercalated cells by principal cells. The recovery could be explained by interconversion of some of the intercalated cells to principal cells. It is also possible that intercalated cells are removed in a similar way as seen in the developing kidney. Here intercalated cells are depleted from the inner medulla by two distinct mechanisms: simple extrusion from the epithelium and by apoptosis followed by phagocytosis by neighboring principal cells during the first 2 wk after birth (21). However, the mechanisms involved in the removal of intercalated cells in kidneys of rats treated for 4 wk with lithium followed by normal diet for 4 wk remains to be established.

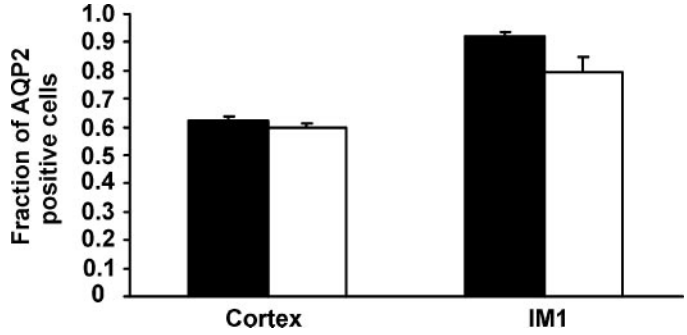

Fig. 14. Quantitation of AQP-2-labeled cells in cortex and IM-1 of control (filled bars) and recovered (open bars) rats. Numbers of AQP-2-positive and -negative cells were determined for kidney sections incubated with anti-AQP-2 and peroxidase-conjugated secondary antibodies. There were no significant differences in the fractions of AQP-2-positive cells between the two groups in cortex and IM-1.

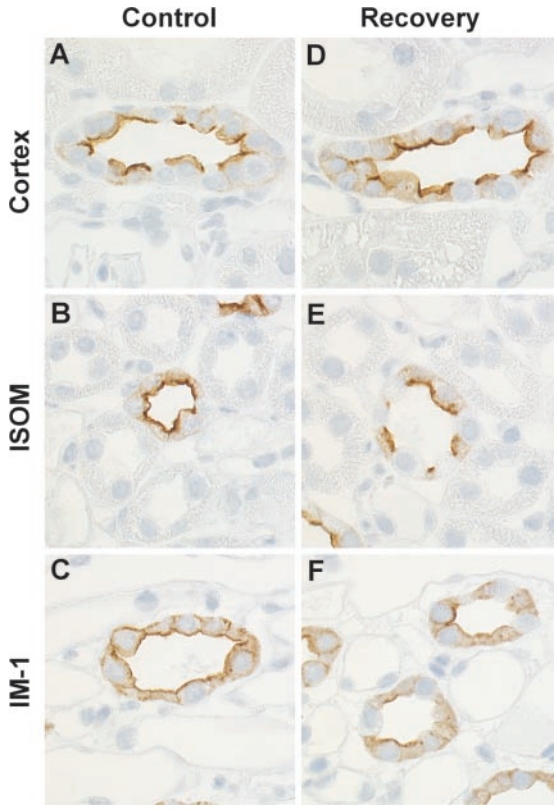

Fig. 13. Immunocytochemistry using whole kidney sections from control rats (*A*-*C*) and rats treated with lithium for 4 wk followed by a 4-wk recovery period (recovery, *D*-*F*). Sections were incubated with anti-AQP-2 antibody and peroxidase-conjugated secondary antibody. Both AQP-2 expression and the density of AQP-2-positive cells were similar in the control and recovery groups. Magnification, ×380.

Summary. This study demonstrated a dramatic change in the composition of cell types in renal collecting ducts in response to prolonged lithium treatment. There is a major decrease in the density of principal cells in parallel with a decrease in AQP-2 expression and an increase in the number of intercalated cells. This may have profound importance for the development of lithium-induced NDI. Moreover, this study raises the possibility that the cellular composition of collecting ducts undergoes substantial modification in response to metabolic changes in the body, which adds another layer of complexity to the web of mechanisms regulating its function.

ACKNOWLEDGMENTS

We thank Lotte V. Holbech, Inger Merete S. Paulsen, Zhila Nikrozi, Mette Vistisen, Ida Maria Jalk, Gitte Kall, and Albert Meyer for expert technical assistance.

GRANTS

Support for this study was provided by the Carlsberg Foundation and the Water and Salt Research Center at the University of Aarhus, which is established and supported by the Danish National Research Foundation (Danmarks Grundforskningsfond). Additional support was provided by the European Commission (Grants QLRT-2000-00987 and QLRT-2000-00778), the Novo Nordisk Foundation (Nordisk Forsknings Komite), Fonden til Lægevidenskabens Fremme, Nyreforeningens Forskningsfond, the Helen and Ejnar Bjørnows Foundation, the Danish Medical Research Council, the Karen Elise Jensen Foundation, and the UK Medical Research Council.

REFERENCES

1. **Aigner J, Kloth S, Jennings ML, and Minuth WW.** Transitional differentiation patterns of principal and intercalated cells during renal collecting duct development. *Epithelial Cell Biol* 4: 121–130, 1995.
2. **Anai H, Ueta Y, Serino R, Nomura M, Kabashima N, Shibuya I, Takasugi M, Nakashima Y, and Yamashita H.** Upregulation of the expression of vasopressin gene in the paraventricular and supraoptic nuclei of the lithium-induced diabetes insipidus rat. *Brain Res* 772: 161–166, 1997.
3. **Bagnis C, Marshansky V, Breton S, and Brown D.** Remodeling the cellular profile of collecting ducts by chronic carbonic anhydrase inhibition. *Am J Physiol Renal Physiol* 280: F437–F448, 2001.
4. **Balment RJ, Jones IC, and Henderson IW.** Time course of lithium-induced alterations in renal and endocrine function in normal and Brattleboro rats with hypothalamic diabetes insipidus. *Br J Pharmacol* 59: 627–634, 1977.
5. **Bucht G and Wahlin A.** Renal concentrating capacity in long-term lithium treatment and after withdrawal of lithium. *Acta Med Scand* 207: 309–314, 1980.
6. **Christensen BM, Wang W, Frøkiær J, and Nielsen S.** Axial heterogeneity in basolateral AQP2 localization in rat kidney: effect of vasopressin. *Am J Physiol Renal Physiol* 284: F701–F717, 2003.
7. **Christensen S.** Vasopressin and renal concentrating ability. In: *Lithium Therapy Monographs*, edited by Johnson FN. Basel: Karger, 1988, vol. 2, p. 20–34.
8. **Dafnis E, Kurtzman NA, and Sabatini S.** Effect of lithium and amiloride on collecting tubule transport enzymes. *J Pharmacol Exp Ther* 261: 701–706, 1992.
9. **Earm JH, Christensen BM, Frøkiær J, Marples D, Han JS, Knepper MA, and Nielsen S.** Decreased aquaporin-2 expression and apical plasma membrane delivery in kidney collecting ducts of polyuric hypercalcemic rats. *J Am Soc Nephrol* 9: 2181–2193, 1998.
10. **Ecelbarger CA, Terris J, Frindt G, Echevarria M, Marples D, Nielsen S, and Knepper MA.** Aquaporin-3 water channel localization and regulation in rat kidney. *Am J Physiol Renal Fluid Electrolyte Physiol* 269: F663–F672, 1995.
11. **Fejes-Toth G and Naray-Fejes-Toth A.** Differentiation of renal beta-intercalated cells to alpha-intercalated and principal cells in culture. *Proc Natl Acad Sci USA* 89: 5487–5491, 1992.
12. **Forrest JN Jr, Cohen AD, Torretti J, Himmelhoch JM, and Epstein FH.** On the mechanism of lithium-induced diabetes insipidus in man and the rat. *J Clin Invest* 53: 1115–1123, 1974.
13. **Frøkiær J, Christensen BM, Marples D, Djurhuus JC, Jensen UB, Knepper MA, and Nielsen S.** Downregulation of aquaporin-2 parallels changes in renal water excretion in unilateral ureteral obstruction. *Am J Physiol Renal Physiol* 273: F213–F223, 1997.
14. **Ghosh PM, Mikhailova M, Bedolla R, and Kreisberg JI.** Arginine vasopressin stimulates mesangial cell proliferation by activating the epidermal growth factor receptor. *Am J Physiol Renal Physiol* 280: F972–F979, 2001.
15. **Gold PW, Robertson GL, Post RM, Kaye W, Ballenger J, Rubinow D, and Goodwin FK.** The effect of lithium on the osmoregulation of arginine vasopressin secretion. *J Clin Endocrinol Metab* 56: 295–299, 1983.
16. **Hemken P, Guo XL, Wang ZQ, Zhang K, and Gluck S.** Immunologic evidence that vacuolar H^+ ATPases with heterogeneous forms of M_r = 31,000 subunit have different membrane distributions in mammalian kidney. *J Biol Chem* 267: 9948–9957, 1992.
17. **Hestbech J, Hansen HE, Amdisen A, and Olsen S.** Chronic renal lesions following long-term treatment with lithium. *Kidney Int* 12: 205–213, 1977.
18. **Jackle T, Hasel C, Melzner I, Bruderlein S, Jehle PM, and Moller P.** Sustained hyposmotic stress induces cell death: apoptosis by defeat. *Am J Physiol Cell Physiol* 281: C1716–C1726, 2001.
19. **Jacobsen NO, Olesen OV, Thomsen K, Ottosen PD, and Olsen S.** Early changes in renal distal convoluted tubules and collecting ducts of lithium-treated rats: light microscopy, enzyme histochemistry, and ^{3}H-thymidine autoradiography. *Lab Invest* 46: 298–305, 1982.
20. **Jamous M, Bidet M, Tauc M, Koechlin N, Gastineau M, Wanstok F, and Poujeol P.** In young primary cultures of rabbit kidney cortical collecting ducts intercalated cells originate from principal or undifferentiated cells. *Eur J Cell Biol* 66: 192–199, 1995.
21. **Kim J, Cha JH, Tisher CC, and Madsen KM.** Role of apoptotic and nonapoptotic cell death in removal of intercalated cells from developing rat kidney. *Am J Physiol Renal Fluid Electrolyte Physiol* 270: F575–F592, 1996.
22. **Kim J, Kim YH, Cha JH, Tisher CC, and Madsen KM.** Intercalated cell subtypes in connecting tubule and cortical collecting duct of rat and mouse. *J Am Soc Nephrol* 10: 1–12, 1999.
23. **Kim YH, Kwon TH, Christensen BM, Nielsen J, Wall SM, Madsen KM, Frøkiær J, and Nielsen S.** Altered expression of renal acid-base transporters in rats with lithium-induced NDI. *Am J Physiol Renal Physiol* 285: F1244–F1257, 2003.
24. **Kim YH, Kwon TH, Frische S, Kim J, Tisher CC, Madsen KM, and Nielsen S.** Immunocytochemical localization of pendrin in intercalated cell subtypes in rat and mouse kidney. *Am J Physiol Renal Physiol* 283: F744–F754, 2002.
25. **Kwon TH, Laursen UH, Marples D, Maunsbach AB, Knepper MA, Frøkiær J, and Nielsen S.** Altered expression of renal AQPs and Na^+ transporters in rats with lithium-induced NDI. *Am J Physiol Renal Physiol* 279: F552–F564, 2000.
26. **Levine S, Saltzman A, and Klein AW.** Proliferation of glial cells in vivo induced in the neural lobe of the rat pituitary by lithium. *Cell Prolif* 33: 203–207, 2000.
27. **Madiehe AM, Mampuru LJ, and Tyobeka EM.** Induction of apoptosis in HL-60 cells by lithium. *Biochem Biophys Res Commun* 209: 768–774, 1995.
28. **Mao CD, Hoang P, and DiCorleto PE.** Lithium inhibits cell cycle progression and induces stabilization of p53 in bovine aortic endothelial cells. *J Biol Chem* 276: 26180–26188, 2001.
29. **Marples D, Christensen S, Christensen EI, Ottosen PD, and Nielsen S.** Lithium-induced downregulation of aquaporin-2 water channel expression in rat kidney medulla. *J Clin Invest* 95: 1838–1845, 1995.
30. **Marples D, Frøkiær J, Dørup J, Knepper MA, and Nielsen S.** Hypokalemia-induced downregulation of aquaporin-2 water channel expression in rat kidney medulla and cortex. *J Clin Invest* 97: 1960–1968, 1996.
31. **Mulders SM, Bichet DG, Rijss JP, Kamsteeg EJ, Arthus MF, Lonergan M, Fujiwara M, Morgan K, Leijendekker R, van der Sluijs P, van Os CH, and Deen PM.** An aquaporin-2 water channel mutant which causes autosomal dominant nephrogenic diabetes insipidus is retained in the Golgi complex. *J Clin Invest* 102: 57–66, 1998.
32. **Nelson RD, Guo XL, Masood K, Brown D, Kalkbrenner M, and Gluck S.** Selectively amplified expression of an isoform of the vacuolar H^+-ATPase 56-kilodalton subunit in renal intercalated cells. *Proc Natl Acad Sci USA* 89: 3541–3545, 1992.
33. **Nielsen S, Pallone T, Smith BL, Christensen EI, Agre P, and Maunsbach AB.** Aquaporin-1 water channels in short and long loop descending thin limbs and in descending vasa recta in rat kidney. *Am J Physiol Renal Fluid Electrolyte Physiol* 268: F1023–F1037, 1995.
34. **Rosenthal W, Seibold A, Antaramian A, Lonergan M, Arthus MF, Hendy GN, Birnbaumer M, and Bichet DG.** Molecular identification of the gene responsible for congenital nephrogenic diabetes insipidus. *Nature* 359: 233–235, 1992.
35. **Sands JM, Flores FX, Kato A, Baum MA, Brown EM, Ward DT, Hebert SC, and Harris HW.** Vasopressin-elicited water and urea permeabilities are altered in IMCD in hypercalcemic rats. *Am J Physiol Renal Physiol* 274: F978–F985, 1998.
36. **Stanton BA and Kaissling B.** Regulation of renal ion transport and cell growth by sodium. *Am J Physiol Renal Fluid Electrolyte Physiol* 257: F1–F10, 1989.
37. **Stone KA.** Lithium-induced nephrogenic diabetes insipidus. *J Am Board Fam Pract* 12: 43–47, 1999.
38. **Sugawara M, Hashimoto K, and Ota Z.** Involvement of prostaglandin E2, cAMP, and vasopressin in lithium-induced polyuria. *Am J Physiol Regul Integr Comp Physiol* 254: R863–R869, 1988.
39. **Terris J, Ecelbarger CA, Nielsen S, and Knepper MA.** Long-term regulation of four renal aquaporins in rats. *Am J Physiol Renal Fluid Electrolyte Physiol* 271: F414–F422, 1996.
40. **Thomsen K.** The effect of sodium chloride on kidney function in rats with lithium intoxication. *Acta Pharmacol Toxicol (Copenh)* 33: 92–102, 1973.
41. **Van Balkom BW, van Raak M, Breton S, Pastor-Soler N, Bouley R, Van Der SP, Brown D, and Deen PM.** Hypertonicity is involved in redirecting the aquaporin-2 water channel into the basolateral, instead of the apical, plasma membrane of renal epithelial cells. *J Biol Chem* 278: 1101–1107, 2003.
42. **Van Os CH and Deen PM.** Aquaporin-2 water channel mutations causing nephrogenic diabetes insipidus. *Proc Assoc Am Physicians* 110: 395–400, 1998.
43. **Zhang Z, Cai Q, Michea L, Dmitrieva NI, Andrews P, and Burg MB.** Proliferation and osmotic tolerance of renal inner medullary epithelial cells in vivo and in cell culture. *Am J Physiol Renal Physiol* 283: F302–F308, 2002.